



Solid-state photochromic molecular switches based on axially chiral and helical spiropyrans

Lang Qu, Xuemei Xu, Jintong Song, Dehua Wu, Lei Wang, Weilan Zhou, Xiangge Zhou, Haifeng Xiang*

College of Chemistry, Sichuan University, Chengdu, 610041, China

ARTICLE INFO

Keywords:

Spiropyran
Chiral BINOL
Molecular switch
Chiroptical
Anticounterfeiting

ABSTRACT

Solid-state photochromic switches with reversible luminescence modulation property have wide applications in optical data storage, anticounterfeiting, sensing, and bioimaging, however, it is a significant challenge to design and prepare such materials. In the present work, a novel class of chiral and helical binaphthyl-substituted spiropyran has been synthesized and characterized. The introduction of binaphthyl can not only promote the solid-state luminescence but also achieve the interesting chiroptical switching properties for the potential applications in chiral recognition and circularly polarized luminescence. The single-crystal structures and density functional theory calculations reveal that the presence of strong electron-withdrawing nitro groups can promote photo-switch efficiency by stabilizing the electron-rich conjugated merocyanine with the lower electron cloud density and LUMO/HOMO levels. For charge transfer in excited states, $\pi \rightarrow \pi^*$ transition would enhance emission, but $n \rightarrow \pi^*$ transition and intramolecular charge transfer show the opposite effect. Therefore, these photochromic switches provide a novel paradigm in the design of multiple-responsive, chiral, and luminescent materials.

1. Introduction

Spiropyran (SP) [1], as one important class of photochromic switches [2], has been extensively investigated in the past two decades due to its versatile applications in optical data storage, anticounterfeiting, sensing, and bioimaging. As shown in Fig. 1, under external stimulus of light, heat, and chemicals, SP switches usually undergo three different isomers including colorless and non-emissive closed-ring SP, purple and red-emissive open-ring merocyanine (MC), and yellow and weakly emissive protonated merocyanine (MCH) [1b]. Previous literature reports have demonstrated that electron-withdrawing groups, such as nitro and methyl pyridinium, can enhance the UV response of photo-switches, because electron-withdrawing groups are known to stabilize the electron-rich conjugated open-ring MC [3]. On the other hand, these electron-withdrawing groups might have tendency to quench the emission [4]. In fact, π -conjugated open-ring MC is planar and consequently far more likely to encounter the problem of emission "aggregation-caused quenching" (ACQ) through intermolecular π - π stacking interactions [5]. Moreover, except the existence of SP-MC photoisomerization, the trans-cis photoisomerization of MC is also reported [6], which would further increase the challenge to design and prepare

SP switches with a high emission quantum yield (Φ).

Organic π -conjugated luminescent materials have attracted great interests in a variety of scientific communities owing to their wide and useful applications [7]. In order to improve Φ of SP switches, many strategies, such as immobilization of the MC moieties into polymer nanoparticles [8] and micelles [9], are adopted to restrict their conformational flexibility and protect the fluorophores from quenching by nonradiative processes. For a chemist, however, a simpler and more efficient and challenging way is to design and synthesize luminescent SP switches through the modification of molecular structures. Recently, to solve the ACQ problem to achieve solid-state luminescence, some popular aggregation-induced emission [5] (AIE)-active moieties, e.g., tetraphenylethene (TPE) [10] and 9,10-distyrylanthracene [11] are combined into SP switches. Furthermore, ACQ-active-pyrene-based SP is demonstrated to exhibit blue-red emission both in solution and in the solid state [12].

1,1'-binaphthyls, 1,1'-binaphthalene-2,2'-diol (BINOL) and 1,1'-binaphthalene-2,2'-diamine (BINAM), are an important class of axially chiral molecules for many applications including supramolecular chemistry [13], asymmetric catalysis [14], enantioselective fluorescent recognition [15], and circularly polarized luminescence (CPL) [16]. To

* Corresponding author.

E-mail address: xianghaifeng@scu.edu.cn (H. Xiang).

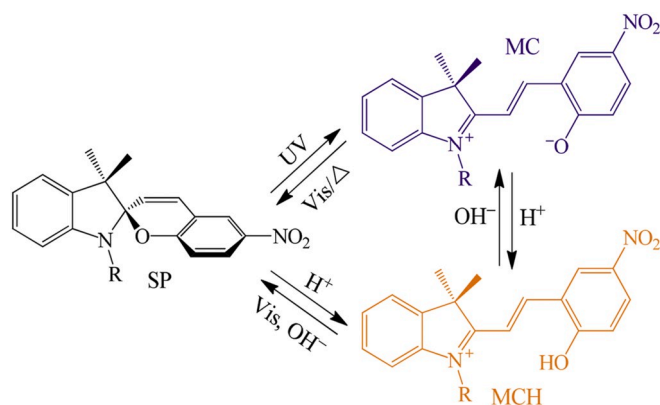


Fig. 1. Photochromism and acidochromism of spiropyran.

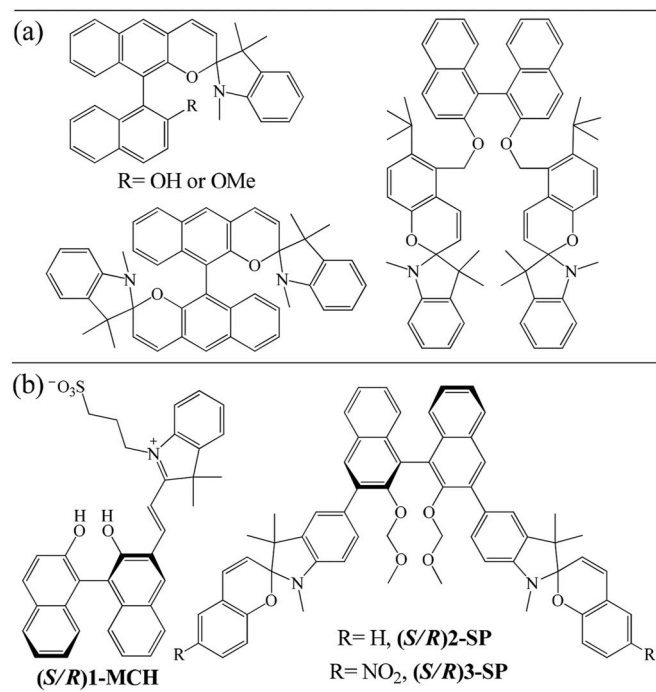


Fig. 2. BINOL-based SP molecules: (a) the previous works; (b) this work.

date, only a limited number of conjugated [17] and un-conjugated [18] BINOL-based SP molecules (Fig. 2a) have been reported for the recognition of amino acids, cations, acid/base. However, owing to the absence of electron-withdrawing groups, there is no report on photochromic transformation from SP to MC under the UV irradiation. Moreover, for these conjugated BINOL-based SP molecules, no luminescent property is demonstrated, which might be caused by the fact that their SP unites are covalently bonded at 2,3-position of BINOL and thus the ring opening of SP might change the dihedral angle between two naphthyl rings and quench the emission consequently. In the present work, combining the axial chirality and AIE property [19] of highly sterically bulky BINOL, we covalently linked SP moieties to BINOL at 3-position to achieve novel photochromic chiral switches, (S/R)1–3 (Fig. 2b), which exhibit highly efficient and reversible solid-state luminescence switching under alternating UV light and heat/visible light treatment.

2. Results and discussion

2.1. Synthesis and characterization

(S/R)1-MCH [20], (S/R)2-SP [21], and (S/R)3-SP [20] were prepared according to three different ways, as shown in Fig. 3. Compound 4 [20], 5 [22], 6 [23], 7 [24], 8 [24] and 9 [25] were prepared according to the previous reports. The best stable form of 1 and 2/3 is MCH [10a] and SP [17,18], respectively. The purpose of the presence of sulfonate group to (S/R)1 is to improve the solubility in water for sensing applications [10a,26]. We failed to prepare pure closed-ring (S/R)1-SP by adding base to (S/R)1-MCH solution, because (S/R)1-SP is salt and thus could not be purified by running chromatography. (S/R)2-SP could be synthesized by Suzuki coupling reaction [21] with a moderate yield of 42%, but (S/R)3-SP could not be obtained by the same way because the electron-withdrawing nitro group would significantly diminish the yield of Suzuki coupling reaction. Therefore, (S/R)3-SP was prepared by a modified way (Fig. 3c). (S/R)1-MCH is soluble in MeOH, DMSO, and DMF rather than CH_2Cl_2 , MeCN, ethyl acetate, and toluene. (S/R)2-SP and (S/R)3-SP are soluble in CH_2Cl_2 , ethyl acetate, THF, DMSO, DMF and toluene rather than MeOH, EtOH, and hexane. We successfully obtained some good-quality single crystals (yellow particles) of (S) 1-MCH (CCDC 1944289) by the vapor diffusion of $\text{CH}_2\text{Cl}_2/\text{MeOH}$. Unfortunately, for (S/R)2-SP and (S/R)3-SP, oil-like thin films were always obtained by various methods. We would like to point out that (S/R)2-SP and (S/R)3-SP with a large molecular weight (924 and 1014) are highly difficult to crystallize.

The photophysical properties, including UV/visible absorption and fluorescence data, of all synthesized (S/R)1–3 at room temperature are listed in Table S1 (in Supporting Information). The photophysical properties, except circular dichroism (CD), of (S) and (R)1–3 are similar, which are consistent with our previous reports [4d,4e,12,16c,16d,27].

2.2. Solution tautomerization properties of (S)1 under base/acid treatments

We first studied the tautomerization properties of (S)1 in solution under base/acid treatments. Density functional theory (DFT) and time-dependent-DFT (TD-DFT) were also performed by Gaussian 09 program package (B3LYP 6-31G(d,p)) to investigate the UV/visible absorption spectra and charge transfer in excited states. NO solid-state tautomerization is found for (S)1. (S)1-SP, (S)1-MC, and (S)1-MCH are non-emissive or weakly emissive in solution or solid.

In dilute DMSO solution, (S)1-MCH exhibits a dominating absorption peak ($\lambda_{\text{abs}} = 425 \text{ nm}$), which is predicted well by theoretical calculation ($\lambda_{\text{abs}} = 416 \text{ nm}$) (Fig. 4e). The optimized molecular structure, energy level diagram, and frontier molecular orbitals of (S)1-MCH are also displayed in Fig. 4a. Unlike our previous report [26a], which demonstrates that the contribution of sulfonate group to the electron cloud density of the highest occupied molecular orbital (HOMO), HOMO-1, the lowest unoccupied molecular orbital (LUMO), and LUMO+1 is relatively small and thus the sulfonate group has little effect on the photophysical properties, the sulfonate group (lone pair electrons of O atoms) of (S)1-MCH has obvious contributions to the electron cloud density of HOMO, HOMO-1, and HOMO-3 (Fig. 4a) due to its electron-rich nature. Moreover, the dihedral angle between the two naphthyl rings of optimized (S)1-MCH is 85.5° (Fig. S1), which indicates that two naphthyl rings are close to vertical and lead to the broken π -conjugation system and the unsymmetrical distribution of electron cloud density [28]. It should be noticed that the lower energy absorption of (S)1-MCH is mainly originated from Excited State 5 (416 nm,

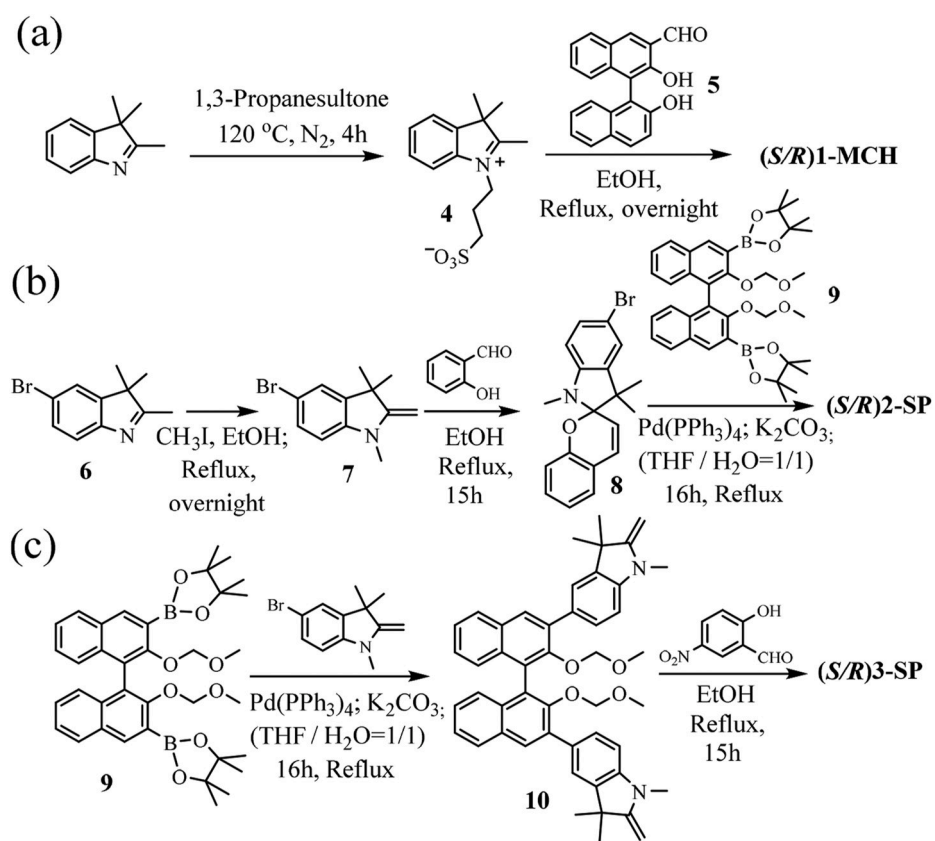


Fig. 3. Synthesis of (S/R)1-3.

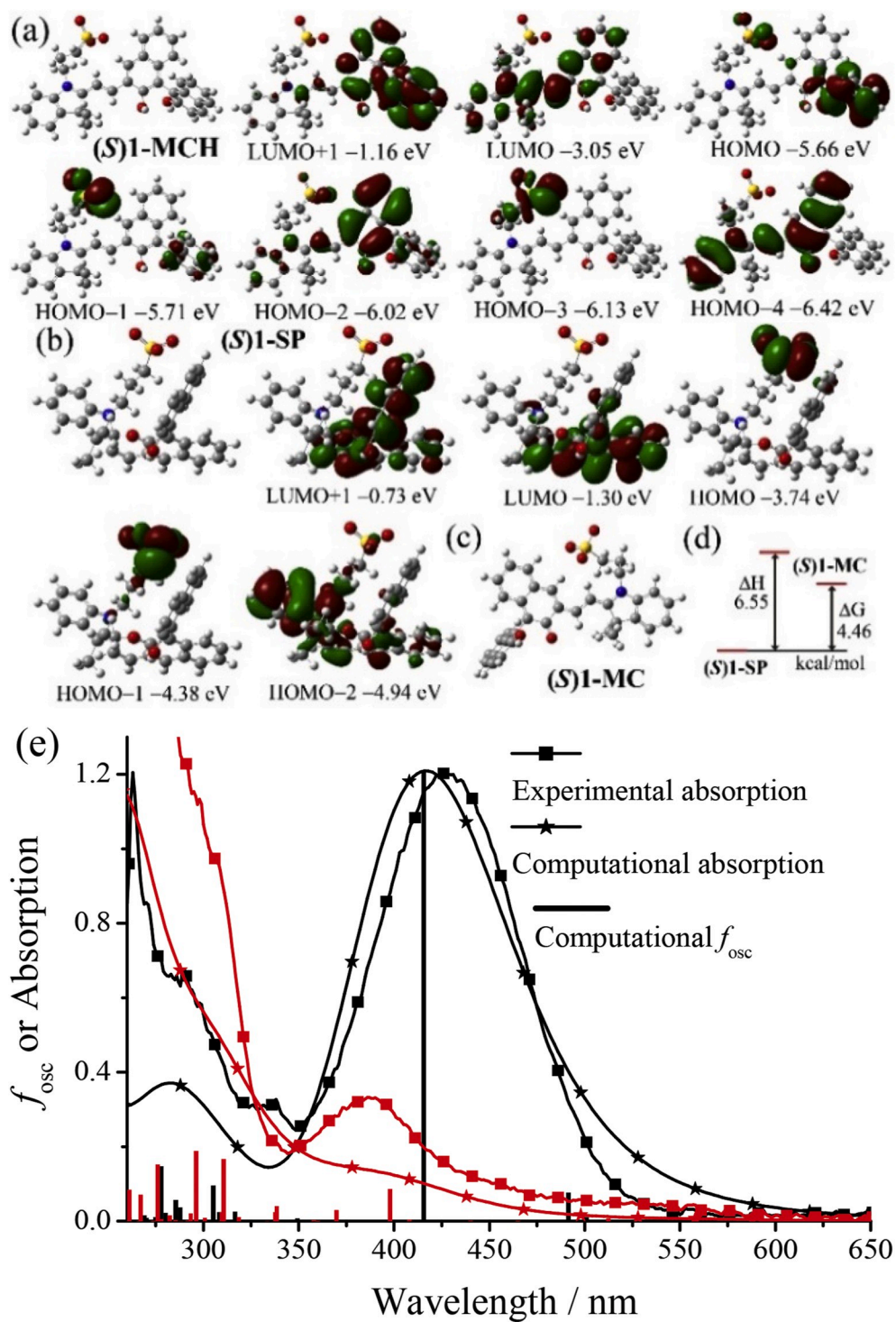


Fig. 4. Computational optimized molecular structures and frontier molecular orbitals of (S)1-MCH (a) and (S)1-SP (b). Computational optimized molecular structure of (S)1-MC (c). Relative enthalpy and free energy levels of (S)1-SP and (S)1-MC (d). Computational and experimental absorption spectra ($10 \mu\text{mol dm}^{-3}$) of (S)1-MCH (black line) and (S)1-SP (red line) in DMSO (e). (For interpretation of the references to color in this figure legend, the reader is referred to the Web version of this article.)

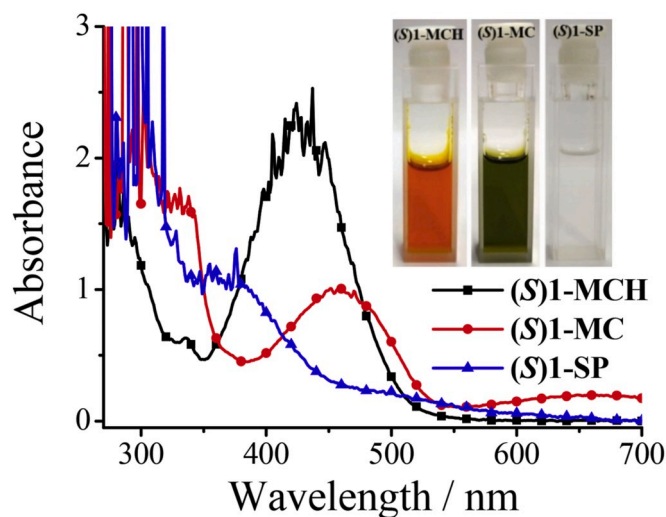


Fig. 5. Absorption spectra and photographs of (S)1-MCH, (S)1-MC ((S)1-MCH upon adding 500 equivalents of NEt_3), and (S)1-SP ((S)1-MCH upon adding 500 equivalents of NaOH) in DMSO (0.1 mmol dm^{-3}).

oscillator strength $f_{\text{osc}} = 0.2203$, HOMO-4 \rightarrow LUMO (92.4%) and HOMO-2 \rightarrow LUMO (6.1%) rather than common Excited State 1 (HOMO \rightarrow LUMO). This might be caused by the facts that (1) HOMO-4 \rightarrow LUMO and HOMO-2 \rightarrow LUMO are the allowable and symmetrical $\pi \rightarrow \pi^*$ transition in the same central π -conjugation of naphthyl-based MCH unit; (2) The level of LUMO+1 (-1.16 eV) is too high for transitions; (3) HOMO \rightarrow LUMO, HOMO-1 \rightarrow LUMO, and HOMO-3 \rightarrow LUMO are involved in asymmetrical $n \rightarrow \pi^*$ and intramolecular charge transfer (ICT).

Upon adding 500 equivalents of NaOH , the yellow DMSO solution of (S)1-MCH will change into colorless (Fig. 4e) immediately, revealing the formation of (S)1-SP ($\lambda_{\text{abs}} = 390 \text{ nm}$) (Fig. 1). This reaction is reversible if HCl acid is added further ((S)1-SP \rightarrow (S)1-MCH). The dihedral angle between the two naphthyl rings of optimized (S)1-SP is 94.9° (Fig. 4b and Fig. S1). It's well-known that SP is non-planar. The dihedral angle between the five-membered pyrrole ring and the six-membered pyran ring is 84.1° for (S)1-SP. By contrast, these units in (S)1-MCH is almost planar. Therefore, the absorption band of (S)1-SP blue shifts into 390 nm , which is mainly contributed to Excited State 6 (398 nm , $f_{\text{osc}} = 0.0858$, HOMO-2 \rightarrow LUMO (97.1%)) with ICT character from the benzopyrrole unit to the naphthyl pyran unit. Owing to the absence of electron-withdrawing groups, no photochromic tautomerization from (S)1-SP into (S)1-MC is observed under the UV irradiation.

In order to trigger to isomerize from (S)1-MCH to (S)1-MC (Fig. 1), NaOH is replaced by a weak base of NEt_3 . When adding 500 equivalents of NEt_3 to a high concentration solution of (S)1-MCH (0.1 mmol dm^{-3}), the orange-yellow solution will change into yellow-green immediately, indicating the possible formation of (S)1-MC (Fig. 5). However, the resultant yellow-green solution is not stable and would change into colorless (S)1-SP in several minutes. The dihedral angle between the two naphthyl rings of optimized (S)1-MC is 75.7° (Fig. 4c and Fig. S1). Indeed, our calculations reveal that the enthalpy (sum of electronic and thermal enthalpies) and free energy (sum of electronic and thermal free energies) between (S)1-SP and (S)1-MC is 6.55 and 4.46 kcal/mol (Fig. 4d), respectively. This indicates that the ring-opening reaction is endothermic and (S)1-SP is thermodynamically more stable than (S)1-MC [29].

2.3. Solution tautomerization properties of (S)2 under base/acid treatments

The dihedral angle between the two naphthyl rings and the pyrrole ring and the pyran ring of optimized (S)2-SP is 87.9° and 88.0° (Fig. 6a and Fig. S1), respectively. Compared with (S)1-SP, (S)2-SP gives a little blue-shifted absorption with a shoulder at $\sim 350 \text{ nm}$ (Fig. S2), which can be classified into Excited State 1 (358 nm , $f_{\text{osc}} = 0.3624$, HOMO \rightarrow LUMO (89.2%), HOMO \rightarrow LUMO+2 (4.5%), HOMO-1 \rightarrow LUMO (2.1%)) with $\pi \rightarrow \pi^*$ character in the naphthyl pyran unit (Fig. 6). Therefore, (S)2-SP emits blue emission (0.6% in MeCN) from naphthyl pyran unit (Table S1 and Fig. S2 and S3) [13e,15]. Moreover, the solid powders ($\Phi = 1.1\%$) and aggregated nanoparticles in THF/ H_2O ($\Phi = 0.5\%$) and MeCN/ H_2O ($\Phi = 1.0\%$) of (S)2-SP show AIE characters (Fig. 7 and Fig. S4). The central rigid BINOL still exhibits intramolecular motions (IMs) [30] through some small-angle rotations around the chiral axis [16c,d]. These IMs would not destroy their chiral configurations but result in emission quenching in a dilute solution. For aggregated nanoparticles and solid powders, however, the IMs would be restricted by the strong intermolecular interactions and thus the emission is enhanced.

Upon adding HCl , the colorless MeOH solution of (S)2-SP will change into yellow (Fig. 6 and Fig. S5) immediately, revealing the formation of (S)2-MCH ($\lambda_{\text{abs}} = 430 \text{ nm}$) (Fig. 1). This reaction is also reversible if NaOH is added further. The dihedral angle between the two naphthyl rings of optimized (S)2-MCH is 120.0° (Fig. 6b and Fig. S1). The absorption band of (S)2-MCH can be mainly contributed to Excited State 3 (499 nm , $f_{\text{osc}} = 0.3592$, HOMO-1 \rightarrow LUMO (92.3%), HOMO-2 \rightarrow LUMO (5.9%)) and 4 (484 nm , $f_{\text{osc}} = 0.5961$, HOMO-2 \rightarrow LUMO+1 (94.6%), HOMO-1 \rightarrow LUMO+1 (3.3%)) with ICT character from the binaphthyl unit to the MCH unit. This ICT character would lead to the absence of emission for (S)2-MCH (Fig. 7). Owing to the absence of electron-withdrawing groups, no photochromic tautomerization from (S)2-SP into (S)2-MC is observed under the UV irradiation.

If 500 equivalents of NEt_3 is added to a high concentration MeOH solution of (S)2-MCH (0.1 mmol dm^{-3}), the orange-yellow solution will change into blue-purple immediately, indicating the possible formation of (S)2-MC. However, the resultant blue-purple solution is highly unstable and will become into colorless (S)2-SP very quickly, and thus we had no time to take the photo and measure the absorption spectrum. The dihedral angle between the two naphthyl rings of optimized (S)2-MC is 119.6° (Fig. 6c and Fig. S1). The enthalpy and free energy between (S)2-SP and (S)2-MC is 14.6 and 9.56 kcal/mol , respectively (Fig. 6d).

2.4. Solution and solid tautomerization properties of (S)3 under base/acid and UV light treatments

The dihedral angle between the two naphthyl rings and the pyrrole ring and the pyran ring of optimized (S)3-SP is 82.4° and 87.5° (Fig. 8a and Fig. S1), respectively. Like (S)2-SP, (S)3-SP shows a similar absorption spectrum with a shoulder at $\sim 350 \text{ nm}$ (Fig. S6). In contrast to that of (S)2-SP, the electron cloud density in LUMO and LUMO+1 of (S)3-SP is mainly located at the nitro groups. The low-energy absorption band of (S)3-SP can be contributed to Excited State 29 (365 nm , $f_{\text{osc}} = 0.2425$, HOMO \rightarrow LUMO+5 (93.5%)) and 30 (351 nm , $f_{\text{osc}} = 0.1218$, HOMO-1 \rightarrow LUMO+5 (96.0%)) with ICT character from the benzopyrrole unit to the naphthyl pyran unit. Therefore, (S)3-SP is non-emissive in solution and solid.

Even upon adding 1000 equivalents of HCl , the colorless MeOH solution of (S)3-SP shows little changes (Fig. 9), revealing the absence of (S)3-MCH (Fig. 1) and the inhibition of chemical switching from the nitro groups. However, if further irradiated by 365 nm UV light for 5

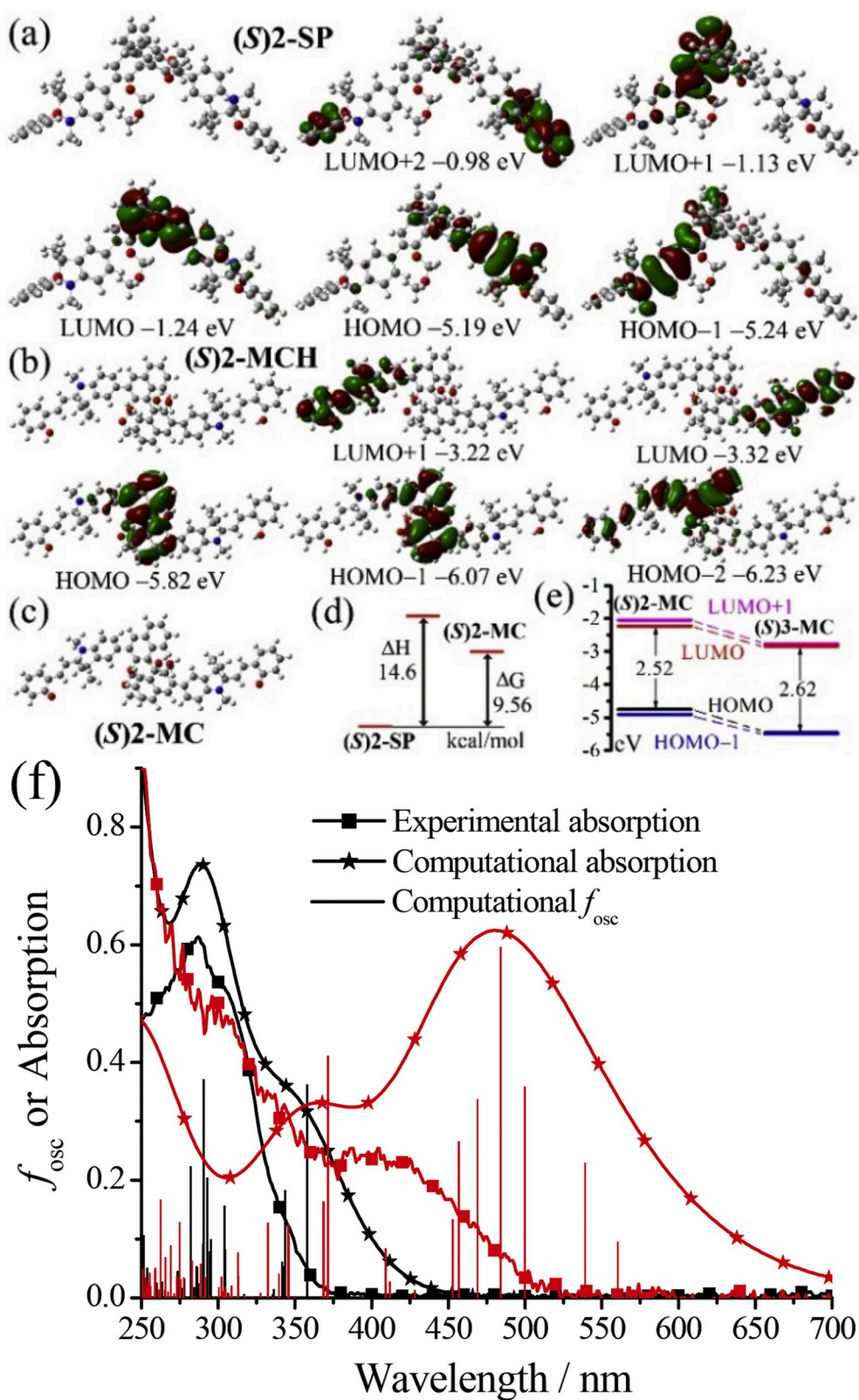


Fig. 6. Computational optimized molecular structures and frontier molecular orbitals of (S)2-SP (a) and (S)2-MCH (b). Computational optimized molecular structure of (S)2-MC (c). Relative enthalpy and free energy levels of (S)2-SP and (S)2-MC (d). Energy level diagram of (S)2-MC and (S)3-MC (e). Computational and experimental absorption spectra ($10 \mu\text{mol dm}^{-3}$) of (S)2-MCH (red line) and (S)2-SP (black line) in MeOH (f). (For interpretation of the references to color in this figure legend, the reader is referred to the Web version of this article.)

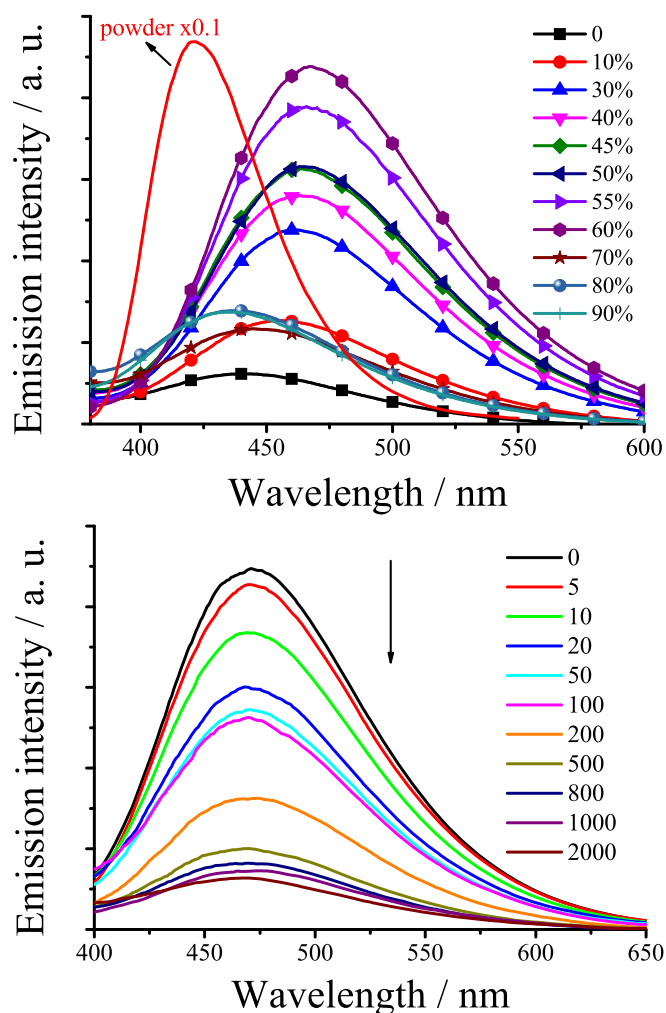


Fig. 7. Top: emission spectra of (S)2-SP in THF/H₂O with different volume fractions of water (f_{water}) ($10 \mu\text{mol dm}^{-3}$) and solid powder (excited at 310 nm). Bottom: emission spectra of (S)2-SP in MeOH ($5 \mu\text{mol dm}^{-3}$) with adding 0 to 2000 equivalents of HCl (excited at 310 nm).

min, the above (S)3-SP solution will change into yellow (S)3-MCH solution ($\lambda_{\text{abs}} = 430 \text{ nm}$). The dihedral angle between the two naphthyl rings of optimized (S)3-MCH is 106.7° (Fig. 8d and Fig. S1). The absorption band of (S)3-MCH can be mainly contributed to Excited State 5 (484 nm , $f_{\text{osc}} = 0.7539$, HOMO-2 \rightarrow LUMO (56.0%), HOMO-3 \rightarrow LUMO (31.8%), HOMO-2 \rightarrow LUMO+1 (9.5%)) with ICT character from the binaphthyl benzopyrrole unit to the MCH unit. This ICT character would lead to the absence of emission for (S)3-MCH as well. Moreover, the nitro groups have no contribution to the electron transitions.

With the help of nitro groups, (S)3-SP in solution exhibits excellent photochromic-switching properties (Fig. 10). When irradiated by 365 nm UV light, the colorless (S)3-SP solution will change into purple, indicating the formation of (S)3-MC. It needs about 10 min UV irradiation to achieve the saturation of purple and the recovery time for colorless solution under sunlight is about 5 min. If heated at 80°C , the purple color will disappear immediately.

Although the ring-opening reaction of (S)3-SP \rightarrow (S)3-MC is endothermic ($\Delta H = 19.2 \text{ kcal/mol}$, Fig. 8c) and heating may help to form (S)3-MC, heating would promote the equilibrium of reaction to yield

thermodynamically stable (S)3-MC ($\Delta G = 16.1 \text{ kcal/mol}$, Fig. 8c). ΔG between (S)3-SP and (S)3-MC is bigger than that between (S)2-SP and (S)2-MC, which is contrary to the fact that the reaction of (S)3-SP \rightarrow (S)3-MC is more efficient than the reaction of (S)2-SP \rightarrow (S)2-MC. The possible reason is that the reaction of SP \rightarrow MC is very complicated and there are some high-energy intermediate compounds [29]. The dihedral angle between the two naphthyl rings of optimized (S)3-MC is 104.1° (Fig. 8b and Fig. S1). The absorption band ($\lambda_{\text{abs}} = 530 \text{ nm}$, Fig. 8e) of (S)3-MC can be mainly contributed to Excited State 1 (531 nm , $f_{\text{osc}} = 1.4867$, HOMO \rightarrow LUMO (91.6%), HOMO-1 \rightarrow LUMO (5.4%), HOMO-1 \rightarrow LUMO+1 (2.2%)) with $\pi \rightarrow \pi^*$ character in the MC unit and nitro group and high f_{osc} . It is unusual that the strong electron-withdrawing nitro groups have contribution to electron cloud density of both HOMO/HOMO-1 and LUMO/LUMO+1 and consequently stabilize the electron-rich conjugated (S)3-MC (Fig. 8b) by reducing the electron cloud density. Moreover, (S)3-MC with nitro groups has a much lower LUMO level of 0.61 eV and HOMO level of 0.71 eV than (S)2-MC (Fig. 6e). Therefore, the above two factors may lead to the efficient photoswitching in (S)3-MC. (S)3-MC is non-emissive in dilute solution and shows weak red AIE in solid powders and aggregated nanoparticles (Table S1 and Fig. S7).

In order to extend the application field in solid state, we doped (S)3-SP into a polymer host of polymethyl methacrylate (PMMA). (S)3-SP-doped PMMA film exhibits excellent photochromic-switching properties as well (Figs. 10 and 11). The transparent and colorless (S)3-SP-doped PMMA film (wt % = 1.0%, thickness = 0.5 mm) will change into purple when irradiated by 365 nm UV light. It needs about 10 min UV irradiation to achieve the saturation of purple and the recovery time for colorless film is about 120 min and 3 min under sunlight and heating at 80°C , respectively. This color change is easily distinguishable by a naked eye. Furthermore, (S)3-SP-doped PMMA film shows good color reversibility and stability against photobleaching.

It is unexpected that, under the UV irradiation, red emission ($\lambda_{\text{abs}} = \sim 640 \text{ nm}$, Fig. S8) from (S)3-MC of PMMA film ($\Phi = 2.2\%$) is much stronger than that of solid powders. Doping technology could reduce not only the IMs but also intermolecular π - π stacking interactions of (S)3-MC. The corresponding fluorescence changes provide a high contrast between turn off and turn on (Fig. 11).

In order to evaluate the conversion efficiency of (S)3-SP \rightarrow (S)3-MC, thin-layer chromatography (TLC) analysis is studied. As shown in Fig. 12, after the elution with ethyl acetate: petroleum ether = 1 : 5, the spot of purple (S)3-MC solution on SiO₂ TLC appears only one colored ribbon under room light (purple), 254 nm UV light (dark), and 365 nm UV light (red), which illustrates that the conversion efficiency is nearly quantitative. The strong absorption at $\sim 590 \text{ nm}$ in MeCN solution and PMMA film further verifies the high conversion efficiency (Fig. 10).

2.5. X-ray single crystal structures

The molecule chemical structures and X-ray single-crystal arrangements of organic materials act an important role in their photophysical properties [4]. In order to investigate the effect of molecule arrangements, the X-ray single-crystal structures of (S)1-MCH are depicted in Fig. 13 and Fig. S9. There is no (R)1-MCH in the X-ray single-crystal structures, which confirms the fact that the (R)/(S)-chiral configurations of BINOL are stable enough for chemical modification. Except one propane-1-sulfonate unit and two methyl groups, other the atoms of (S)1-MCH are located in two planes: one is peripheral naphthyl ring, the other is naphthyl-based MCH. The dihedral angle between the two naphthyl rings in X-ray single-crystal structure (75.2°) is smaller than that in optimized structure (85.5°), revealing that the binaphthyl exhibits the IMs through a rotation around the chiral axis in gas state or

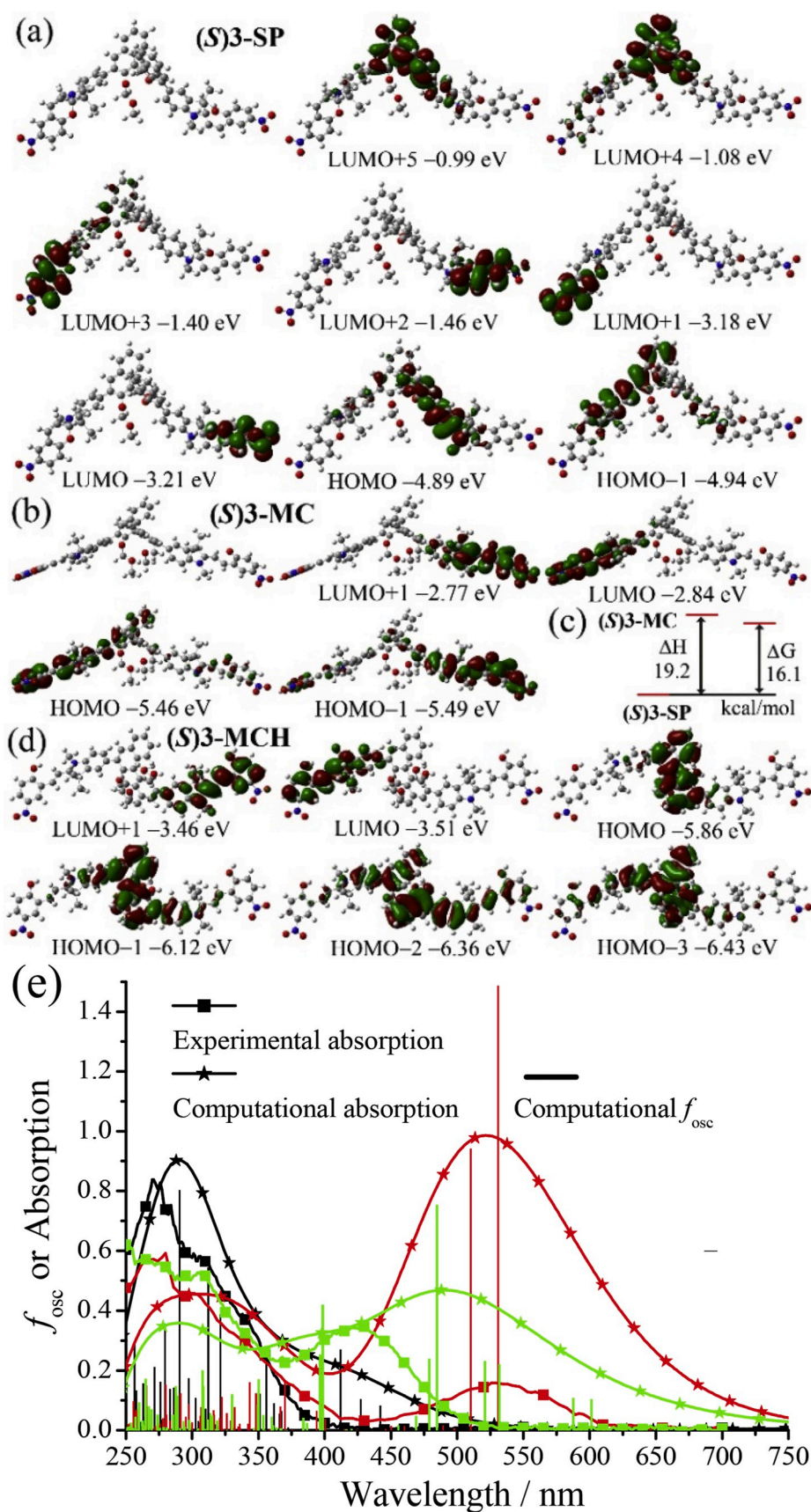


Fig. 8. Computational molecular structures and frontier molecular orbitals of (S)3-SP (a), (S)3-MC (b), and (S)3-MCH (d). Relative enthalpy and free energy levels of (S)3-SP and (S)3-MC (c). Computational and experimental absorption spectra ($10 \mu\text{mol dm}^{-3}$) of (S)3-SP (back line), (S)3-MC (red line), and (S)3-MCH (green line) in MeOH (e). (For interpretation of the references to color in this figure legend, the reader is referred to the Web version of this article.)

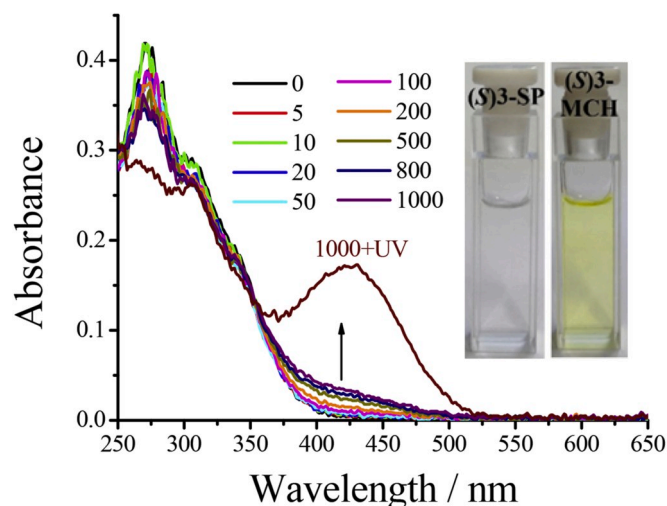


Fig. 9. Absorption spectra of (S)3-SP ($5 \mu\text{mol dm}^{-3}$) in MeOH with adding 0 to 1000 equivalents of HCl. Absorption spectrum of (S)3-SP ($10 \mu\text{mol dm}^{-3}$) in MeOH with adding 1000 equivalents of HCl and 5 min UV irradiation. Insert: photographs of (S)3.

dilute solution [16c,d]. Although (S)1-MCH is propeller-type, some intermolecular π - π stacking interactions are still observed in its X-ray single-crystal structures (Fig. S9) [31]. Furthermore, many strong intermolecular interactions including hydrogen bond O...H (1.895 Å), S...H (2.323 Å), and H...H (2.197 Å) are found between the neighboring (S)1-MCH molecules. These strong intermolecular interactions could eliminate the IMs and help to self-assemble (S)1-MCH molecules to build 1-D hierarchical helices of helices (helical pitch = 22.3 Å) in one crystal cell, which indicate that these materials might be superior in the CPL switching application [16].

2.6. Chiroptical properties

The chirality properties of (R/S)2-SP and (R/S)3-SP in dilute MeCN solution and PMMA are investigated by CD spectra (Fig. 14). Even in dilute MeCN, the CD signals of (R/S)2-SP and (R/S)3-SP are still strong. (S)2-SP, the (S) enantiomer, shows positive Cotton peak at 270 nm and negative Cotton peaks at 236, 289, and 340 nm. (R)2-SP, the (R) enantiomer, exhibits exactly the mirrored CD spectrum indicating that (S)2-SP and (R)2-SP are a pair of enantiomers. The similar phenomena are observed for (S)3-SP and (R)3-SP enantiomers. Combining with previous work [13e,16c,d,32], the CD signals are mainly originated from chiral binaphthyl itself.

Since (R/S)3-SP exhibits excellent photochromic-switching properties, its chiroptical-switching properties are examined in both dilute solution and PMMA film (Fig. 14). It is unexpected that, when irradiated (R/S)3-SP solution by 365 nm UV light for 10 min, the resultant purple (R/S)3-MC solution do not show any Cotton peak in longer wavelength regions (>400 nm). This indicates that (R/S)3-MC has strong absorption at longer wavelength regions, but the responsive CD signals are much lower compared to those in shorter wavelength regions [17b,33] and might be caused by the fact that the absorption of (R/S)3-MC at longer wavelength regions is mainly originated from $\pi \rightarrow \pi^*$ character in the MC unit and nitro group and the central chiral binaphthyl unit has little contribution. For PMMA film, however, the Cotton peak around 590 nm is still weak but detectable.

2.7. Thermochromism

Thermochromism denotes the phenomenon of a color change with dependence on temperature [34]. As shown in Fig. 15, when (S)3-MC in MeCN solution is cooled to 77 K in liquid nitrogen, the purple color will

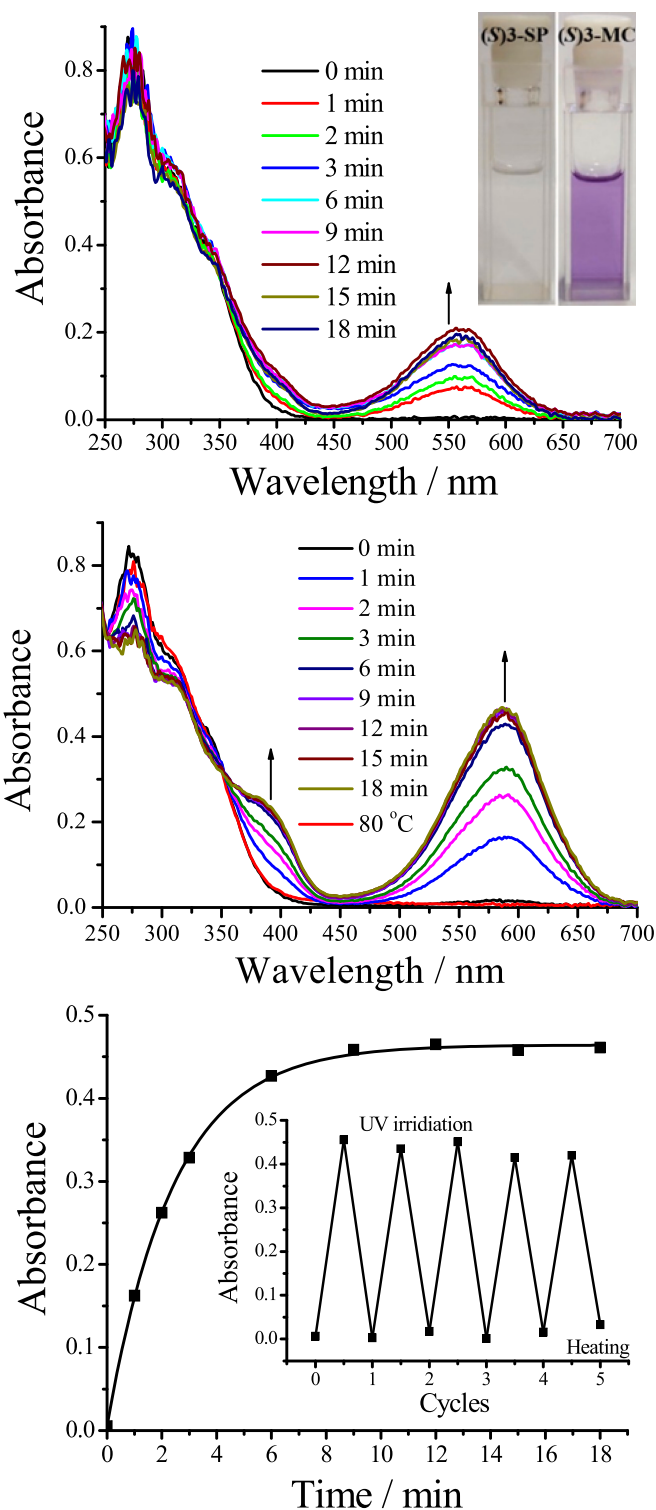


Fig. 10. Top: absorption spectra changes of (S)3-SP ($10 \mu\text{mol dm}^{-3}$) in MeCN upon irradiation with 365 nm UV light. Insert: photographs of (S)3. Middle: absorption spectra changes of (S)3-SP-doped (wt % = 1.0%) PMMA film upon irradiation with 365 nm UV light and the recovery under heating at 80 °C. Bottom: absorption dynamics at the peak (590 nm) of the (S)3-SP-doped (wt % = 1.0%) PMMA film when exposed to continuous 365 nm UV irradiation. Insert: its absorbance contrast profiles under 365 nm UV irradiation and heating (80 °C) treatment with switching cycles.

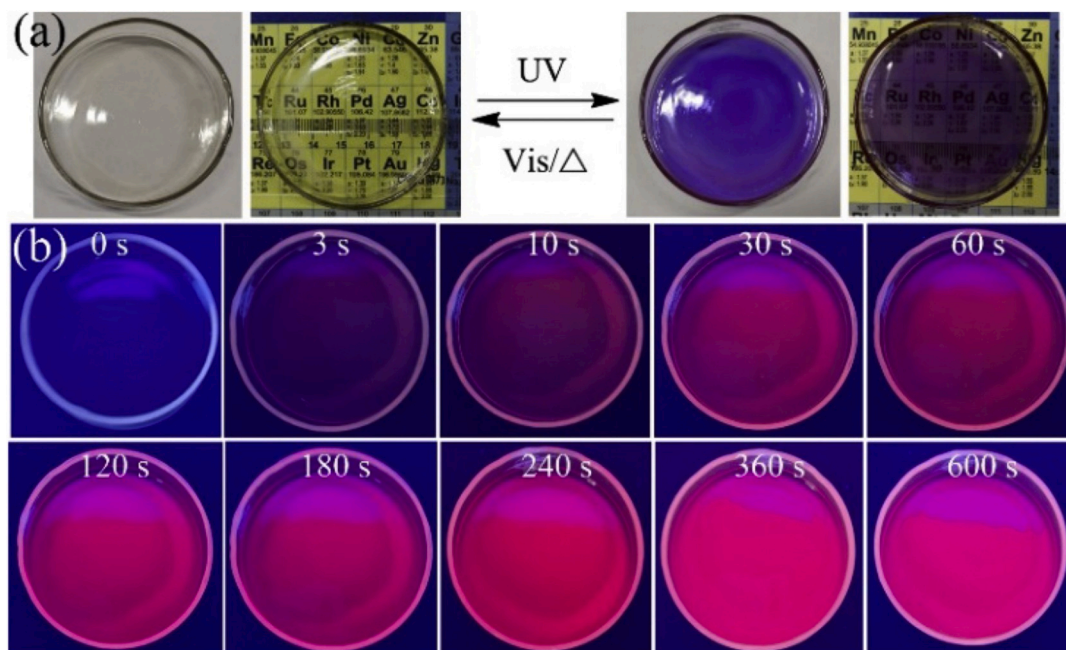


Fig. 11. Absorption spectra changes of (S)3-SP-doped (wt % = 1.0%) PMMA film (thickness = 0.5 mm) upon irradiation with 365 nm UV light and the recovery under heating at 80 °C.

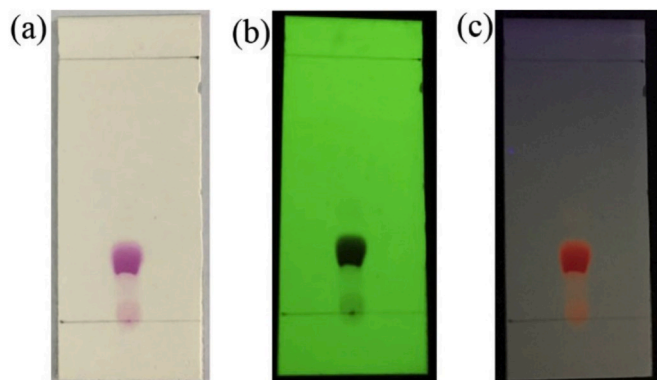


Fig. 12. Photographs of (S)3-SP (MeCN solution upon irradiation with 10 min 365 nm UV light) on SiO₂ TLC using ethyl acetate: petroleum ether = 1:5 as eluent (a: under room light; b: under 254 nm UV light; c: under 365 nm UV light).

change into orange-red color. When temperature is increased to room temperature, the color will recover to purple color and finally become colorless. This color change is reversible and visible to the naked eyes. As previously mentioned, the ring-opening reaction of (S)3-SP → (S)3-MC is endothermic, and thus cooling would help to form colorless (S)3-SP from purple (S)3-MC. Consequently, the color of frozen mixture will change from purple into orange-red color.

2.8. Anticounterfeiting mark

The counterfeiting of good and money has important economic implications and is also a threat to health and security [35]. Turn-on fluorescence is widely adopted for a normal anticounterfeiting mark, when it was irradiated by UV light. If (S)3-SP-doped PMMA film (wt % = 1.0%) is used as anticounterfeiting mark, it is possible to provide more usefully signal changes for counterfeiting. As shown in Figs. 11 and 16, combining photoetching technology, (S)3-SP can be used as a promising

anticounterfeit mask with both visual color (colorless ↔ continuously increased purple) and fluorescence (dark ↔ continuously increased red) changes under room light and UV light, respectively.

3. Conclusions

In summary, we have prepared and reported a unique serial of binaphthyl-substituted spiropyran, which show not only the interesting chiroptical switching properties but also the solid-state luminescence. The introduction of strong electron-withdrawing nitro groups would help to promote photochromic switching but hinder chemical switching. The nitro groups can stabilize the electron-rich conjugated merocyanine with the lower LUMO and HOMO levels. Therefore, these multi-stimuli-responsive molecular switches have potential applications in not only optical data storage, anticounterfeiting, sensing, and bioimaging but also chiral recognition and circularly polarized luminescence.

4. Experimental section

4.1. Materials and instrumentation

All reagents were purchased from commercial suppliers and used without further purification. ¹H NMR (400 MHz) spectra were recorded in DMSO-*d*₆. Chemical shifts are reported in ppm using tetramethylsilane as internal standard. UV/vis absorption spectra were recorded using a U5100 (Hitachi) spectrophotometer with quartz cuvettes of 1 and 0.1 cm pathlength for solution and PMMA film, respectively. Fluorescence spectra were obtained using F-7000 Fluorescence spectrophotometer (Hitachi) at room temperature. The slit width was 5 nm and 2.5 nm for excitation and emission. The photon multiplier voltage was 400 V. CD spectra were recorded using a Chirascan plus qCD (Applied Photophysics) at room temperature. HR-MS were obtained with a Waters-Q-TOF-Premier (electrospray ionization mass spectrometry, ESI).

4.2. Measurement of fluorescence quantum yield (Φ)

The quantum yield of a solution sample was measured by the optical

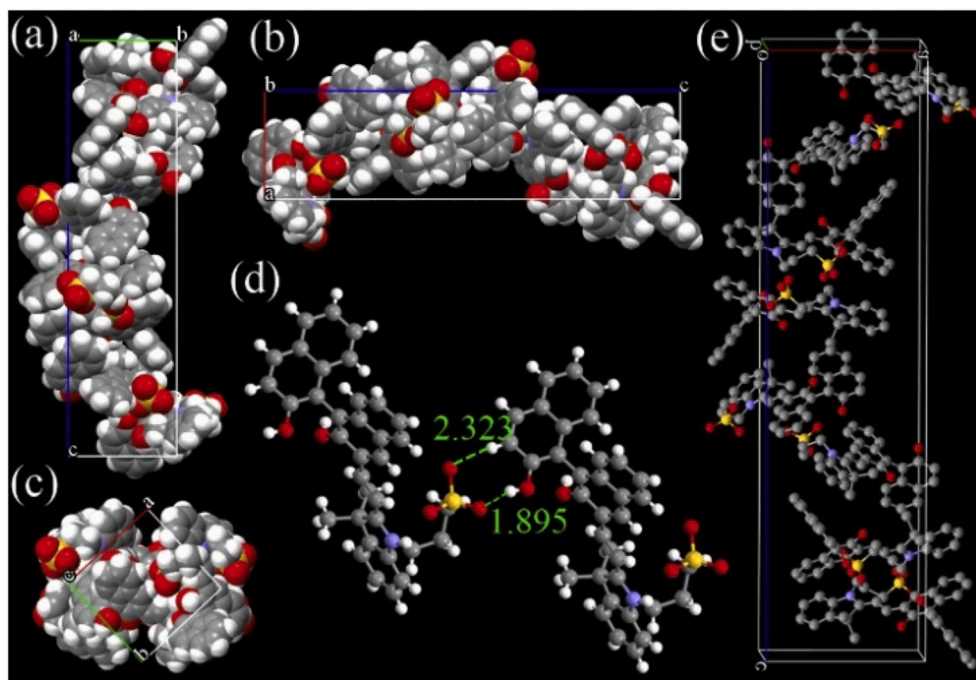


Fig. 13. X-ray single crystal structures and packing of (S)1-MCH molecules: packing in a unit cell from a view down the crystallographic a (a), b (b and e), and c (c) axes; intermolecular interactions (d). H atoms are omitted in (e).

dilute method of Demas and Crosby with a standard of quinine sulfate ($\Phi_r = 0.55$, quinine in 0.05 mol dm⁻³ sulfuric acid) calculated by: $\Phi_s = \Phi_r(B_r/B_s)(n_s/n_r)^2(D_s/D_r)$, where the subscripts s and r refer to the sample and reference standard solution respectively; n is the refractive index of the solvents; D is the integrated intensity. The excitation intensity B is calculated by: $B = 1 - 10^{-AL}$, where A is the absorbance at the excitation wavelength and L is the optical path length (L = 1 cm in all cases). The refractive indices of the solvents at room temperature are taken from standard source. The quantum yield of a solid sample was measured by an integrating sphere.

4.3. X-ray crystallographic analysis

The determination of the unit cell and data collection for four single crystal samples were performed on a Xcalibur E X-ray single crystal diffractometer equipped with graphite monochromator Mo K α ($\lambda = 0.71073$ Å) radiation. The data collection was executed using CrysAlisPro program. Structures were solved by direct method and successive Fourier difference syntheses (SHELXS-97), and were refined by full matrix least-squares procedure on F2 with anisotropic thermal parameters for all nonhydrogen atoms (SHELXL-97).

4.4. Computational details

Calculations were carried out using the Gaussian 09 software package [B3LYP 6-31G(d,p)] based on the X-ray single-crystal structure or its modified structures. The ground state geometry was optimized using DFT. The excited states were predicted using the ground state geometry using TD-DFT, from where UV/Vis absorption (pcm method for solvent effect; 100 excited states) were predicted.

4.4.1. Synthesis of (R/S)1-MC

7 (1.41 g, 5.0 mmol) and **8** (0.63 g, 2.0 mmol) were added into anhydrous ethanol (30 mL), and then the mixture was allowed to reflux overnight. The organic solid was filtered, and then the precipitate was washed with EtOH afford to a dark yellowish brown solid (0.76 g, 66%). ¹H NMR (400 MHz, DMSO-*d*₆) δ 9.52 (s, 1H), 9.26 (d, *J* = 11.1 Hz, 2H), 8.82 (d, *J* = 16.3 Hz, 1H), 8.26 (d, *J* = 16.3 Hz, 1H), 8.08 (d, *J* = 7.9 Hz, 2H), 7.97–7.85 (m, 3H), 7.69–7.59 (m, 2H), 7.37 (dd, *J* = 7.8, 5.7 Hz, 2H), 7.29 (ddd, *J* = 14.8, 8.2, 1.1 Hz, 2H), 7.25–7.19 (m, 1H), 6.96 (d, *J* = 8.3 Hz, 1H), 6.87 (d, *J* = 8.3 Hz, 1H), 5.01–4.87 (m, 2H), 2.78–2.69 (m, 2H), 2.28 (s, 2H), 1.82 (s, 6H). ¹³C NMR (101 MHz, DMSO-*d*₆) δ 181.75, 154.04, 151.83, 149.64, 143.73, 140.99, 136.83, 134.22, 131.64, 130.06, 129.96, 129.87, 129.48, 129.44, 129.28, 129.09, 128.71, 128.42, 128.22, 126.42, 124.63, 123.93, 123.12, 122.58, 118.86, 118.03, 115.28, 113.52, 112.98, 52.09, 47.44, 45.73, 39.52, 26.29, 24.81. HR-MS (ESI): *m/z*: calcd: 577.1923; found: 578.1998 [M+H]⁺, 600.1840 [M+Na]⁺.

4.4.2. Synthesis of (R/S)2-SP

(R/S)-**4** (1.88 g, 3.0 mmol), **3** (2.14 g, 6.0 mmol), and Cs₂CO₃ (4.90 g, 15.0 mmol) were transferred into a round-bottom flask, which was full of nitrogen gas. 30 mL THF and 6 mL distilled water were injected into the flask. When the solution was stirred uniformly and frozen with liquid nitrogen, Pd(PPh₃)₄ (0.16 g) was added. The contents of the flask were evaporated, and nitrogen was pumped for three cycles to replace the residual oxygen. After the solution melted and the temperature returned to room temperature, the reaction liquid was heated to reflux for 16 h. Then, 60 mL water was added into the flask, and the solution was extracted three times with ethyl ether. The organic layer was combined and dried with anhydrous sodium sulfate. Then, the solvent was evaporated, and crude product was obtained. The crude product

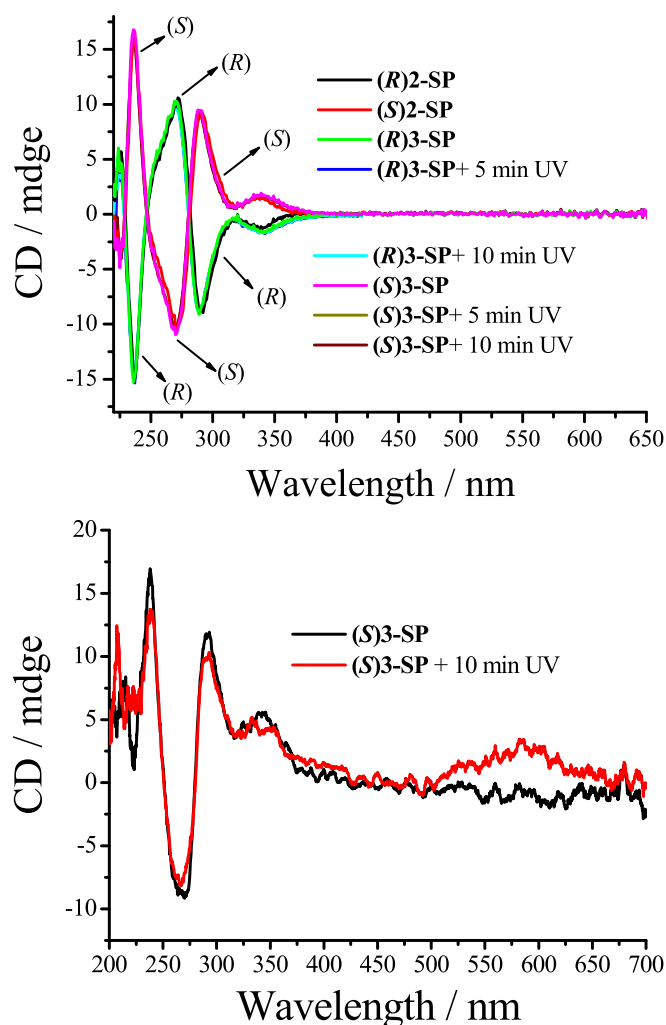


Fig. 14. Top: CD spectra of (*R/S*)2-SP and (*R/S*)3-SP (without and with 5 min and 10 min UV irradiation) in MeCN ($5 \mu\text{mol dm}^{-3}$). Bottom: CD spectra of (*S*)3-SP-doped PMMA film (wt % = 1.0%) without and with 10 min UV irradiation.

was purified by flash column chromatography (ethyl acetate: petroleum ether = 1 : 100~1 : 25) to give target compound (*R/S*)2-SP (1.16 g, 42%) as a white amorphous solid. ^1H NMR (400 MHz, $\text{DMSO-}d_6$) δ 8.12–7.99 (m, 4H), 7.52–7.42 (m, 6H), 7.29 (t, $J = 7.6$ Hz, 2H), 7.18 (d, $J = 7.4$ Hz, 2H), 7.14–7.06 (m, 4H), 7.03 (d, $J = 10.2$ Hz, 2H), 6.84 (td, $J = 7.4, 2.7$ Hz, 2H), 6.68 (dd, $J = 14.8, 7.6$ Hz, 4H), 5.79 (d, $J = 10.2$ Hz, 2H), 4.50–4.41 (m, 2H), 4.34 (td, $J = 5.4, 2.7$ Hz, 2H), 2.71 (s, 6H), 2.39 (s, 6H), 1.29–1.23 (m, 6H), 1.15 (s, 6H). ^{13}C NMR (101 MHz, $\text{DMSO-}d_6$) δ 153.89, 150.65, 147.31, 136.52, 135.59, 132.59, 130.63, 129.78, 129.38, 129.09, 128.79, 127.90, 126.92, 125.91, 125.59, 125.01, 122.51, 120.23, 119.02, 118.58, 114.30, 106.69, 103.98, 97.46, 55.43, 51.39, 30.95, 28.58, 25.54, 22.06, 19.85. HR-MS (ESI): m/z : calcd: 924.4138; found: 925.4216 [$\text{M}+\text{H}$] $^+$, 947.3998 [$\text{M}+\text{Na}$] $^+$.

4.4.3. Synthesis of (*R/S*)3-SP

(*R/S*)-4 (3.76 g, 6.0 mmol), 2 (4.40 g, 15.4 mmol), and Cs_2CO_3 (10.0 g, 30.7 mmol) were transferred into a round-bottom flask, which was full of nitrogen. 60 mL THF and 12 mL distilled water were injected into the flask. When the solution was stirred uniformly and frozen with liquid nitrogen, $\text{Pd}(\text{PPh}_3)_4$ (0.33 g) was added. The contents of the flask were evaporated, and nitrogen was pumped for three cycles to replace

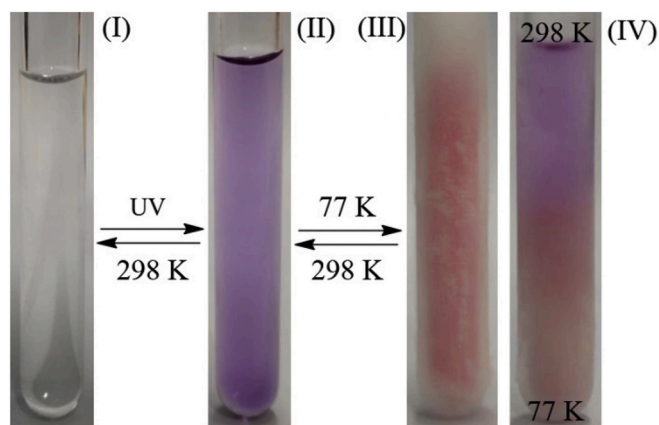


Fig. 15. Photographs of (*S*)3-SP in MeCN ($5 \mu\text{mol dm}^{-3}$) at room temperature (I and II) or 77 K (III: whole was cooled by liquid nitrogen; IV: half bottom was cooled by liquid nitrogen).

the residual oxygen. After the solution melted and the temperature returned to room temperature, the reaction liquid was heated to reflux for 18 h. Then, 100 mL water was added into the flask, and the solution was extracted three times with ethyl ether. The organic layer was combined and dried with anhydrous sodium sulfate. Then, the solvent was evaporated, and crude product was obtained. The crude product was purified by flash column chromatography (ethyl acetate: petroleum ether = 1 : 1) to give target compound 5 a reddish brown oil. The reddish brown oily liquid was taken out of the solvent in vacuo to give a light purple solid (1.69 g, 52%). This product was used directly in the next step without further purification. The crude organic 5 (1.69 g, 2.36 mmol), 5-nitrosalicylaldehyde (1.00 g, 6.14 mmol) and anhydrous EtOH (150 mL) were added into a flask. The reaction solution under a nitrogen atmosphere was heated to reflux for 48 h. Then, the solvent was evaporated to obtain a red powder as a crude product. The crude compound was purified by column chromatography (ethyl acetate: Petroleum ether = 1 : 10) to afford a pale green powder solid (1.41 g, 58%). ^1H NMR (400 MHz, $\text{DMSO-}d_6$) δ 8.25–8.23 (m, 2H), 8.07 (d, $J = 2.0$ Hz, 2H), 8.02 (ddd, $J = 7.8, 6.7, 2.9$ Hz, 4H), 7.49 (d, $J = 9.6$ Hz, 4H), 7.44 (d, $J = 7.9$ Hz, 2H), 7.30 (t, $J = 7.6$ Hz, 2H), 7.26 (d, $J = 10.3$ Hz, 2H), 7.12–7.05 (m, 2H), 6.92–6.87 (m, 2H), 6.77 (d, $J = 7.9$ Hz, 2H), 6.03 (d, $J = 10.5$ Hz, 2H), 4.47 (t, $J = 5.0$ Hz, 1H), 4.42 (dd, $J = 5.2, 2.4$ Hz, 1H), 4.35–4.30 (m, 2H), 2.74 (s, 6H), 2.39 (dd, $J = 6.2, 2.0$ Hz, 6H), 1.27 (d, $J = 12.5$ Hz, 6H), 1.18 (d, $J = 7.1$ Hz, 6H). ^{13}C NMR (101 MHz, $\text{DMSO-}d_6$) δ 159.31, 150.62, 146.87, 140.53, 135.98, 135.49, 132.63, 130.61, 129.61, 128.98, 128.36, 127.94, 126.06, 125.88, 125.75, 125.57, 125.06, 122.83, 122.63, 121.24, 118.90, 115.32, 106.24, 97.50, 55.45, 51.93, 30.95, 28.54, 25.58, 22.05, 19.58. HR-MS (ESI): m/z : calcd: 1014.3840; found: 1015.3921 [$\text{M}+\text{H}$] $^+$, 1037.3720 [$\text{M}+\text{Na}$] $^+$.

Declaration of competing interest

There are no conflicts to declare.

CRediT authorship contribution statement

Lang Qu: Investigation, Formal analysis, Visualization, Writing - original draft. **Xuemei Xu:** Writing - original draft. **Jintong Song:** Conceptualization, Methodology. **Dehua Wu:** Conceptualization, Methodology. **Lei Wang:** Investigation. **Weilan Zhou:** Validation. **Xiangge Zhou:** Methodology. **Haifeng Xiang:** Resources, Supervision, Writing - original draft.

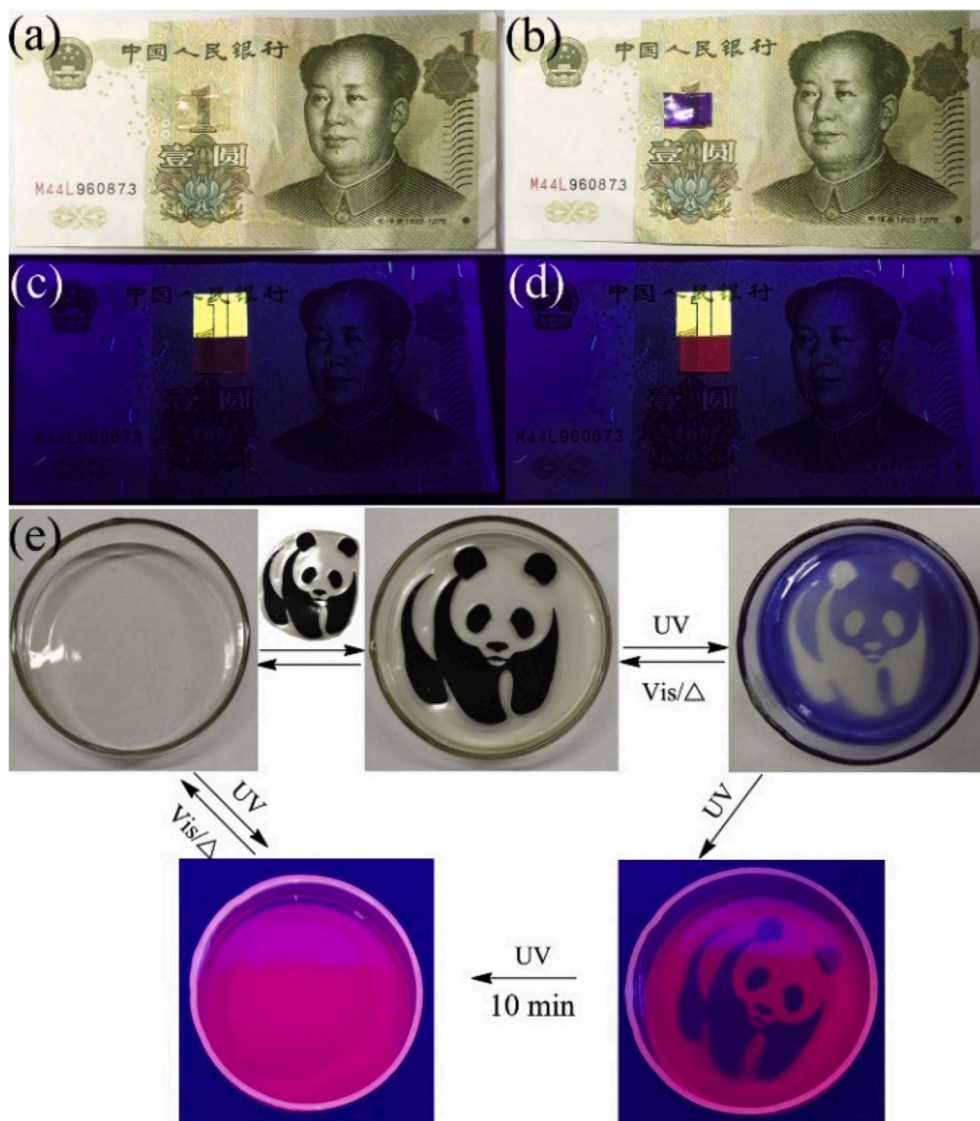


Fig. 16. Photographs of (S)3-SP-doped (wt % = 1.0%) PMMA film (thickness = 0.5 mm) on 1 yuan RMB without (a) and with 0.5 min (c) and 10 min (b,d) UV irradiation under room light or UV light. The PMMA film with panda shielding mask under room light or UV light (e).

Acknowledgements

This work was supported by the National Natural Science Foundation of China (no. 21871192) and Sichuan Science and Technology Program (no. 2018JY0559). We acknowledge the comprehensive training platform of the specialized laboratory of the College of Chemistry, Sichuan University, for material analysis. We would like to thank the Analytical & Testing Center of Sichuan University for CCD X-ray single crystal diffractometer work and circular dichroism spectrometer work. We are grateful to Daibing Luo and Yani Xie for help with the single crystal and circular dichroism measurements.

Appendix A. Supplementary data

Supplementary data related to this article can be found at <https://doi.org/10.1016/j.dyepig.2020.108597>.

References

- [1] (a) Berkovic G, Krongauz V, Weiss V. Spiroprans and spirooxazines for memories and switches. *Chem Rev* 2000;100:1741–54.(b) Klajn R. Spiropyran-based dynamic materials. *Chem Soc Rev* 2014;43:148–84.
- [2] (a) Feringa BL, van Delden RA, Koumura N, Geertsema EM. Chiroptical molecular switches. *Chem Rev* 2000;100:1789–816.(b) Russev MM, Hecht S. Photoswitches: from molecules to materials. *Adv Mater* 2010;22:3348–60.(c) Ko CC, Yam VWW. Transition metal complexes with photochromic ligands-photosensitization and photoswitchable properties. *J Mater Chem* 2010;20:2063–70.(d) Natali M, Giordani S. Molecular switches as photocontrollable “smart” receptors. *Chem Soc Rev* 2012;41:4010–29.(e) Szymański W, Beierle JM, Kistemaker HA, Velema VWA, Feringa BL. Reversible photocontrol of biological systems by the incorporation of molecular photoswitches. *Chem Rev* 2013;113:6114–78.(f) Zhang J, Wang J, Tian H. Taking orders from light: progress in photochromic bio-materials. *Mater Horiz* 2014;1:169–84.(g) Isla H, Crassous J. Helicene-based chiroptical switches. *C R Chimie* 2016;19:39–49.(h) Wang L, Li Q. Photochromism into nanosystems: towards lighting up the future nanoworld. *Chem Soc Rev* 2018;47:1044–97.(i) Ko CC, Yam VWW. Coordination compounds with photochromic ligands: ready tunability and visible light-sensitized photochromism. *Acc Chem Res* 2018;51:149–59.
- [3] (a) Bénard S, Yu P. New spiroprans showing crystalline-state photochromism. *Adv Mater* 2000;12:48–50.(b) Nadir N, Wahid Z, Zainuddin MT, Islam NZM. Photochromic behavior of spiroprans: the effect of substituent. *Adv Mater Res* 2014;925:323–8.(c) Balmond EI, Tautges BK, Faulkner AL, Or VW, Hodur BM, Shaw JT, Louie AY. Comparative evaluation of substituent effect on the photochromic properties of spiroprans and spirooxazines. *J Org Chem* 2016;81:8744–58.(d) Shiozaki H. Molecular orbital calculations for acid induced ring opening reaction of spiropran. *Dyes Pigments* 1997;33(3):229–37.
- [4] (a) Ma XF, Cheng JH, Liu JY, Zhou XG, Xiang HF. Ratiometric fluorescent pH probes based on aggregation-induced emission-active salicylaldehyde azines. *New J Chem* 2015;39:492–500.(b) Cheng JH, Li YX, Sun R, Liu JY, Gou F, Zhou XG, Xiang HF, Liu J. Functionalized Salen ligands linking with non-conjugated bridges:

- unique and colorful aggregation-induced emission, mechanism, and applications. *J Mater Chem C* 2015;3:11099–110. (c) Zhang XH, Shen GY, Gou F, Cheng JH, Zhou XG, Xiang HF. Non-conjugated fluorescent molecular cages of salicylaldehyde-based tri-Schiff bases: AIE, enantiomers, mechanochromism, anion hosts/probes, and cell imaging properties. *Mater Chem Front* 2017;1:1041–50. (d) Shen GY, Gou F, Cheng JH, Zhang XH, Zhou XG, Xiang HF. Chiral and non-conjugated fluorescent salen ligands: AIE, anion probes, chiral recognition of unprotected amino acids, and cell imaging applications. *RSC Adv* 2017;7:40640–9. (e) Wang M, Cheng CQ, Song JT, Wang J, Zhou XG, Xiang HF, Liu J. Multiple hydrogen bonds promoted ESIPt and AIE-active chiral salicylaldehyde hydrazone. *Chin J Chem* 2018;36:698–707.
- [5] (a) Birks JB. *Photophysics of aromatic molecules*. Wiley; 1970. (b) Ma XF, Sun R, Cheng JH, Liu JY, Gou F, Xiang HF, Zhou XG. Fluorescence aggregation-caused quenching versus aggregation-induced emission: a visual teaching technology for undergraduate chemistry students. *J Chem Educ* 2016;93:345–50. (c) Hong Y, Lam JWY, Tang BZ. Aggregation-induced emission. *Chem Soc Rev* 2011;40:5361–88. (d) Mei J, Leung NLC, Kwok RTK, Lam JWY, Tang BZ. Aggregation-induced emission: together we shine, united we soar! *Chem Rev* 2015;115:11718–940.
- [6] (a) Fleming CL, Li S, Grötl M, Andréasson J. Shining new light on the spiropyran photoswitch: a photocage decides between cis–trans or spiro-merocyanine isomerization. *J Am Chem Soc* 2018;140:14069–72. (b) Ma ZY, Meng X, Ji YJ, Li AS, Qi GY, Xu WQ, Zou B, Ma YG, Kuang GC, Jia XR. Pressure induced the largest emission wavelength change in a single crystal. *Dyes Pigments* 2019;162:136–44. (c) Bao BW, Bai SA, Fan J, Su JH, Wang W, Yu D. A novel and durable photochromic cotton-based fabric prepared via thiolene click chemistry. *Dyes Pigments* 2019;171:107778.
- [7] (a) Valeur B. *Molecular fluorescence: principles and applications*. Wiley; 2002. (b) Mitschke U, Bauerle P. The electroluminescence of organic materials. *J Mater Chem* 2000;10:1471–507. (c) Mullen K, Scherf U. *Organic light emitting devices—synthesis, properties and applications*. Wiley; 2006. (d) In: Yersin H, editor. *Highly efficient OLEDs with phosphorescent materials*. Wiley; 2007. (e) Xiang HF, Cheng JH, Ma XF, Zhou XG, Chroma JJ. Near-infrared phosphorescence: materials and applications. *Chem Soc Rev* 2013;42:6128–85. (f) Zhang JF, Zhou Y, Yoon J, Kim JS. Recent progress in fluorescent and colorimetric chemosensors for detection of precious metal ions (silver, gold and platinum ions). *Chem Soc Rev* 2011;40:3416–29. (g) Kaur K, Saini R, Kumar A, Luxami V, Kaur N, Singh P. Chemodosimeters: an approach for detection and estimation of biologically and medically relevant metal ions, anions and thiols. *Coord Chem Rev* 2012;256:1992–2028. (h) Feng Y, Cheng JH, Zhou L, Zhou XG, Xiang HF. Ratiometric optical oxygen sensing: a review in respect of material design. *Analyst* 2012;137:4885–901. (i) Yang YM, Zhao Q, Feng W, Li FY. Luminescent chemodosimeters for bioimaging. *Chem Rev* 2013;113:192–270. (j) Cheng JH, Zhou XG, Xiang HF. Fluorescent metal ion chemosensors via cation exchange reactions of complexes, quantum dots, and metal–organic frameworks. *Analyst* 2015;140:7082–115.
- [8] (a) Zhu MQ, Zhu LY, Han JJ, Wu WW, Hurst JK, Li ADQ. Spiropyran-based photochromic polymer nanoparticles with optically switchable luminescence. *J Am Chem Soc* 2006;128:4303–9. (b) Chan YH, Gallina ME, Zhang X, Wu IC, Jin Y, Sun W, Chiu DT. Reversible photoswitching of spiropyran-conjugated semiconducting polymer dots. *Anal Chem* 2012;84:9431–8. (c) Chen J, Wang D, Turshatov A, Munoz-Espi R, Ziener U, Koynov K, Landfester K. One-pot fabrication of amphiphilic photoswitchable thiophene-based fluorescent polymer dots. *Polym Chem* 2013;4:773–81.
- [9] (a) Chen J, Zeng F, Wu SZ, Zhao JQ, Chen QM, Tong Z. Reversible fluorescence modulation through energy transfer with ABC triblock copolymer micelles as scaffolds. *Chem Commun* 2008:5580–2. (b) Huang CQ, Wang Y, Hong CY, Pan CY. Spiropyran-based polymeric vesicles: preparation and photochromic properties. *Macromol Rapid Commun* 2011;32:1174–9.
- [10] (a) Yu Q, Su X, Zhang T, Zhang YM, Li M, Liu Y, Zhang SXA. Non-invasive fluorescence switch in polymer films based on spiropyran-photoacid modified TPE. *J Mater Chem C* 2018;6:2113–22. (b) Lin T, Su X, Wang K, Li M, Guo H, Liu L, Zou B, Zhang YM, Liu Y, Zhang SXA. An AIE fluorescent switch with multi-stimuli responsive properties and applications for quantitatively detecting pH value, sulfite anion and hydrostatic pressure. *Mater Chem Front* 2019;3:1052–61.
- [11] Qi Q, Li C, Liu X, Jiang S, Xu Z, Lee R, Zhu M, Xu B, Tian W. Solid-state photoinduced luminescence switch for advanced anticounterfeiting and super-resolution imaging applications. *J Am Chem Soc* 2017;139:16036–9.
- [12] Su X, Ji Y, Pan W, Chen S, Zhang YM, Lin T, Liu L, Li M, Liu Y, Zhang SXA. Pyrene spiropyran dyad: solvato-, acido- and mechanofluorochromic properties and its application in acid sensing and reversible fluorescent display. *J Mater Chem C* 2018;6:6940–8.
- [13] (a) Liu M, Zhang L, Wang T. Supramolecular chirality in self-assembled systems. *Chem Rev* 2015;115:7304–97. (b) Chen LJ, Yang HB, Shionoya M. Chiral metallosupramolecular architectures. *Chem Soc Rev* 2017;46:2555–76. (c) Tam AYY, Yam VWW. Recent advances in metallo-gels. *Chem Soc Rev* 2013;42:1540–67. (d) Babu SS, Praveen VK, Ajayaghosh A. Functional π -gelators and their applications. *Chem Rev* 2014;114:1973–2129. (e) Xu XM, Qu L, Song JT, Wu DH, Zhou XG, Xiang HF. A simple and visual approach for enantioselective recognition through supramolecular gels with specific selectivity. *Chem Commun* 2019;55:9873–6.
- [14] Kocovsky P, Vyskocil S, Smrcina M. Non-symmetrically substituted 1,1'-binaphthyls in enantioselective catalysis. *Chem Rev* 2003;103:3213–46.
- [15] (a) Pu L. Fluorescence of organic molecules in chiral recognition. *Chem Rev* 2004;104:1687–716. (b) Hembury GA, Borovkov VV, Inoue Y. Chirality-sensing supramolecular systems. *Chem Rev* 2008;108:1–73. (c) Pu L. Enantioselective fluorescent sensors: a tale of BINOL. *Acc Chem Res* 2012;45:150–63. (d) Zhang X, Yin J, Yoon J. Recent advances in development of chiral fluorescent and colorimetric sensors. *Chem Rev* 2014;114:4918–59. (e) You L, Zha D, Anslvyn EV. Recent advances in supramolecular analytical chemistry using optical sensing. *Chem Rev* 2015;115:7840–92. (f) Pu L. Simultaneous determination of concentration and enantiomeric composition in fluorescent sensing. *Acc Chem Res* 2017;50:1032–40. (g) Keum SR, Lee MJ, Swansburg S, Buncelb E, Lemieux RP. Resolution and circular dichroism of a non-activated spiropyran dye: 6-(p-Chlorophenylazo)-10,30,30-trimethylspiro[2H-1-benzopyran-2,20-indoline]. *Dyes Pigments* 1998;39(4):383–8.
- [16] (a) Sanchez-Carnerero EM, Agarrabeitia AR, Moreno F, Maroto BL, Muller G, Ortiz MJ, delMoya S. Circularly polarized luminescence from simple organic molecules. *Chem Eur J* 2015;21:13488–500. (b) Kumar J, Nakashima T, Kawai T. Circularly polarized luminescence in chiral molecules and supramolecular assemblies. *J Phys Chem Lett* 2015;6:3445–52. (c) Song JT, Wang M, Zhou XG, Xiang HF. Unusual circularly polarized and aggregation-induced near-infrared phosphorescence of helical platinum(II) complexes with tetradentate salen ligands. *Chem Eur J* 2018;24:7128–32. (d) Song JT, Wang M, Xu XM, Qu L, Zhou XG, Xiang HF. 1D-helical platinum(II) complexes bearing metal-induced chirality, aggregation-induced red phosphorescence, and circularly polarized luminescence. *Dalton Trans* 2019;48:4420–8.
- [17] (a) Tsubaki K, Mukoyoshi K, Morikawa HI, Kinoshita T, Fuji K. Enantiomeric recognition of amino acids using a chiral spiropyran derivative. *Chirality* 2002;14:713–5. (b) Zhou Y, Zhang D, Zhang Y, Tang Y, Zhu D. Tuning the CD spectrum and optical rotation value of a new binaphthalene molecule with two spiropyran units: mimicking the function of a molecular “AND” logic gate and a new chiral molecular switch. *J Org Chem* 2005;70:6164–70. (c) É Kőszegi, Grün A, Bitter I. 1,1'-Binaphtho(aza)crowns carrying photochromic signalling unit, I: synthesis, characterization and cation recognition properties. *Supramol Chem* 2006;18:67–76.
- [18] Shao N, Jin J, Wang H, Zheng J, Yang R, Chan W, Abliz Z. Design of bis-spiropyran ligands as dipolar molecule receptors and application to in vivo glutathione fluorescent probes. *J Am Chem Soc* 2010;132:725–36.
- [19] (a) Song F, Xu Z, Zhang Q, Zhao Z, Zhang H, Zhao W, Qiu Z, Qi C, Zhang H, Sung HHY, Williams ID, Lam JWY, Zhao Z, Qin A, Ma D, Tang BZ. Highly efficient circularly polarized electroluminescence from aggregation-induced emission luminogens with amplified chirality and delayed fluorescence. *Adv Funct Mater* 2018;28:1800051. (b) Wang YC, Hu LL, Zhao F, Yu SS, Tian J, Shi D, Wang XJ, Yu XQ, Pu L. Polymer amplified enantioselectivity in the fluorescent recognition of prolinol. *Chem Eur J* 2017;23:17678–81. (c) Li X, Hu W, Wang Y, Quan Y, Cheng Y. Strong CPL of achiral AIE-active dyes induced by supramolecular self-assembly in chiral nematic liquid crystals (AIE-N^{*}-LCs). *Chem Commun* 2019;55:5179–82. (d) Zhang X, Zhang Y, Li Y, Quan Y, Cheng Y, Li Y. High brightness circularly polarized blue emission from non-doped OLEDs based on chiral binaphthyl-pyrene emitters. *Chem Commun* 2019;55:9845–8.
- [20] Shi Z, Peng P, Strohecker D, Liao Y. Long-lived photoacid based upon a photochromic reaction. *J Am Chem Soc* 2011;133:14699–703.
- [21] Suzuki A. Carbon-carbon bonding made easy. *Chem Commun* 2005:4759–63.
- [22] Bougachi M, Watanabe S, Arai T, Sasai H, Shibasaki M. Catalytic asymmetric epoxidation of α,β -unsaturated ketones promoted by lanthanoid complexes. *J Am Chem Soc* 1997;119:2329–30.
- [23] Oriou J, Ng F, Hadziioannou G, Garbay G, Bousquet M, Vignau L, Cloutet E, Brochon C. Synthesis of squaraine-based alternated π -conjugated copolymers: from conventional cross-coupling reactions to metal-free polycondensation. *Polym Chem* 2014;5:7100–8.
- [24] (a) Kundu PK, Olsen GL, Kiss V, Klajn R. Nanoporous frameworks exhibiting multiple stimuli responsiveness. *Nat Commun* 2014;5:3588. (b) Kundu PK, Lerner A, Kucanda K, Leitun G, Klajn R. Cyclic kinetics during thermal equilibration of an axially chiral bis-spiropyran. *J Am Chem Soc* 2014;136(32):11276–9. (c) Zhu MQ, Zhang GF, Hu Z, Aldred MP, Li C, Gong WL, Chen T, Huang ZL, Liu SY. Reversible fluorescence switching of spiropyran-conjugated biodegradable nanoparticles for super-resolution fluorescence imaging. *Macromolecules* 2014;47:1543–52.
- [25] Matsunaga S, Das J, Roels J, Vogl EM, Yamamoto N, Iida T, Yamaguchi K, Shibasaki M. The first optically active BINOL–BINAP copolymer Catalyst: highly stereoselective tandem asymmetric reactions. *J Am Chem Soc* 2000;122:6500–1.
- [26] (a) Zhou L, Cai PY, Feng Y, Cheng JH, Xiang HF, Liu J, Wu D, Zhou XG. Synthesis and photophysical properties of water-soluble sulfonato-Salen-type Schiff bases and their applications of fluorescence sensors for Cu²⁺ in water and living cells. *Anal Chim Acta* 2012;735:96–106. (b) Chen S, Hong Y, Liu Y, Liu J, Leung CWT, Li M, Kwok RTK, Zhao E, Lam JWY, Yu Y, Tang BZ. Full-range intracellular pH sensing by an aggregation-induced emission-active two-channel ratiometric fluorogen. *J Am Chem Soc* 2013;135:4926–9. (c) Cheng JH, Ma XF, Zhang YH, Liu JY, Zhou XG, Xiang HF. Optical chemosensors based on transmetalation of salen-based schiff base complexes. *Inorg Chem* 2014;53:3210–9. (d) Cheng JH, Gou F, Zhang XH, Shen GY, Zhou XG, Xiang HF. A class of multiresponsive colorimetric and fluorescent pH probes via three different reaction mechanisms of salen complexes: a selective and accurate pH measurement. *Inorg Chem* 2016;55:9221–9.
- [27] Qu L, Li CB, Shen GY, Gou F, Song JT, Wang M, Xu XM, Zhou XG, Xiang HF. Syntheses, crystal structures, chirality and aggregation-induced phosphorescence of stacked binuclear platinum(II) complexes with bridging Salen ligands. *Mater Chem Front* 2019;3:1199–209.
- [28] Wang M, Cheng CQ, Li CB, Wu DH, Song JT, Wang J, Zhou XG, Xiang HF, Liu J. Smart, chiral, and nonconjugated cyclohexane-based bis-salicylaldehyde hydrazides: multi-stimuli-responsive, turn-on, ratiometric, and thermochromic

- fluorescence, single-crystal structures via DFT calculations. *J Mater Chem C* 2019; 7:6767–78.
- [29] (a) Cottone G, Noto R, Manna GL, Fornili SL. Ab initio study on the photoisomers of a nitro-substituted spiroopyran. *Chem Phys Lett* 2000;319:51–9.(b) Cottone G, Noto R, Manna GL, Fornili SL. Theoretical study of spiroopyran–merocyanine thermal isomerization. *Chem Phys Lett* 2004;388:218–22.(c) Liu CG, Guan XH. Redox and photoisomerization switching of the second-order optical nonlinearity of a tetrathiafulvalene derivative of spiroopyran across five states: a DFT study. *Phys Chem Chem Phys* 2012;14:5297–306.(d) Lee BH, Jaung JY. Synthesis and characteristics of dicyanopyrazine dyes containing spiroopyran group. *Dyes Pigments* 2003;59:135–42.
- [30] Leung NLC, Xie N, Yuan W, Liu Y, Wu Q, Peng Q, Miao Q, Lam JWY, Tang BZ. Restriction of intramolecular motions: the general mechanism behind aggregation-induced emission. *Chem Eur J* 2014;20:15349–53.
- [31] Gou F, Cheng JH, Zhang XH, Shen GY, Zhou XG, Xiang HF. Unusual aggregation/gelation-induced phosphorescence of propeller-type binuclear platinum(II) enantiomers. *Eur J Inorg Chem* 2016:4862–6.
- [32] Berova N, Di Bari L, Pescitelli G. Application of electronic circular dichroism in configurational and conformational analysis of organic compounds. *Chem Soc Rev* 2007;36:914–31.
- [33] Chaolumen, Ito H, Itami K. An axially chiral 1,1'-biazulene and its π -extended derivative: synthesis, structures and properties. *Chem Commun* 2019;55:9606–9.
- [34] (a) Seeboth A, Löttsch D, Ruhmann R, Muehling O. Thermochromic polymers-function by design. *Chem Rev* 2014;114:3037–68.(b) Rajamalli P, Gandeepan P, Huang MJ, Cheng CH. Bromo induced reversible distinct color switching of a structurally simple donor–acceptor molecule by vapo, piezo and thermal stimuli. *J Mater Chem C* 2015;3:3329–35.
- [35] Arppe R, Sørensen TJ. Physical unclonable functions generated through chemical methods for anti-counterfeiting. *Nat Rev Chem* 2017;1:31.